# Calibration of Fe XANES for high-precision determination of Fe oxidation state in glasses: Comparison of new and existing results obtained at different synchrotron radiation sources

ADRIAN FIEGE<sup>1,\*</sup>, PHILIPP RUPRECHT<sup>2</sup>, ADAM C. SIMON<sup>1</sup>, AARON S. BELL<sup>3</sup>, JÖRG GÖTTLICHER<sup>4</sup>, MATT NEWVILLE<sup>5</sup>, TONY LANZIROTTI<sup>5</sup>, AND GORDON MOORE<sup>1</sup>

<sup>1</sup>Department of Earth and Environmental Sciences, University of Michigan, 1100 North University Avenue Ann Arbor, Michigan 48109-1005, U.S.A.
<sup>2</sup>Lamont-Doherty Earth Observatory, Columbia University, 61 Route 9W, Palisades, New York 10964-8000, U.S.A.
<sup>3</sup>Institute of Meteoritics, University of New Mexico, 221 Yale Blouvard N.E., Albuquerque, New Mexico 87131, U.S.A.
<sup>4</sup>ANKA Synchrotron Radiation Facility, Karlsruhe Institute of Technology, Hermann-von-Helmholtz-Platz 1, 76344 Eggenstein-Leopoldshafen, Germany
<sup>5</sup>Advanced Photon Source (APS), Argonne National Laboratory, Building 401, 9700 S. Cass Avenue, Argonne, Illinois 60439, U.S.A.

#### **ABSTRACT**

Micro-X-ray absorption near-edge structure ( $\mu$ -XANES) spectroscopy has been used by several recent studies to determine the oxidation state and coordination of iron in silicate glasses. Here, we present new results from Fe  $\mu$ -XANES analyses on a set of 19 Fe-bearing felsic glasses and 9 basaltic glasses with known, independently determined, iron oxidation state. Some of these glasses were measured previously via Fe XANES (7 rhyolitic, 9 basaltic glasses; Cottrell et al. 2009), while most felsic reference glasses (12) were analyzed for the first time. The main purpose of this study was to understand how small changes in glass composition, especially at the evolved end of silicate melt compositions occurring in nature, may affect a calibration of the Fe  $\mu$ -XANES method.

We performed Fe  $\mu$ -XANES analyses at different synchrotron radiation sources [Advanced Photon Source (APS), Argonne, U.S.A., and Angströmquelle Karlsruhe (ANKA), Germany] and compared our results to existing calibrations obtained at other synchrotron radiation sources worldwide. The compiled results revealed that changes in instrumentation have a negligible effect on the correlation between the centroid energy of the Fe pre-edge peak and the Fe oxidation state in the glasses. Oxidation of the glasses during extended exposure (up to 50 min) to the X-ray beam was not observed.

Based on the new results and literature data we determined a set of equations for different glass compositions, which can be applied for the calculation of the iron valence ratio (Fe³+/ $\Sigma$ Fe) in glasses by using XANES spectra collected at different synchrotron beamlines. For instance, the compiled felsic reference material data demonstrated that the correlation between the centroid energy of the Fe pre-edge peak  $C_{Fe}$  (eV) and the Fe³+/ $\Sigma$ Fe ratio of felsic glasses containing 60.9 to 77.5 wt% SiO<sub>2</sub> and 1.3 to 5.7 wt% FeO<sub>tot</sub> can be accurately described by a single linear trend, if the spectra were collected at 13-ID-E beamline at APS and for  $0.3 \le Fe³+/\Sigma Fe \le 0.85$ :

 $C_{Fe}$  [eV] = 0.012395 (±0.00026217) × Fe<sup>3+</sup>/ $\Sigma$ Fe + 7112.1 (±0.014525); R<sup>2</sup> = 0.987.

Based on this equation, the Fe oxidation state of felsic glasses can be estimated at an absolute uncertainty of  $\pm 2.4\%$  Fe<sup>3+</sup>/ $\Sigma$ Fe.

In general, the differences between the calibrations for felsic and mafic glasses were small and the compiled data set (i.e., results collected at four different beamlines on 79 reference glass materials) is well described by a single second-order polynomial equation.

**Keywords:** Fe micro-XANES, synchrotron radiation sources/beamlines, Fe oxidation state, Fe coordination, silicate glasses, rhyolite, dacite, basalt

# INTRODUCTION

Iron (Fe) is by far the most abundant element in geological compounds that exhibits variable valence states (Fe<sup>0</sup>, Fe<sup>2+</sup>, and Fe<sup>3+</sup>), with total FeO (FeO<sub>tot</sub>) contents ranging from <1 wt% in evolved felsic magmas to >10 wt% in basaltic systems (e.g.,

Condie 1993; Hofmann 1988; O'Connor 1965; Wilke et al. 2005). Considering that a wide range of Fe³+/ $\Sigma$ Fe is realized in magmatic systems (e.g., Fe³+/ $\Sigma$ Fe increases from ~0.1 at QFM-1 to 0.5–0.7 at QFM+4; Kress and Carmichael 1991; Moretti 2005), Fe is often the main carrier of the redox budget of a magma and is as ferric or ferrous iron in oxides (e.g., spinel) and silicates (e.g., olivine, pyroxene) participating in various (solid) buffer reactions in nature. The valence state of Fe in silicate melts is heavily dependent on the oxygen fugacity ( $f_{02}$ ), but

<sup>\*</sup> Present address: Department of Earth and Planetary Sciences, American Museum of Natural History, Central Park West at 79th Street, New York, NY 10024-5192, U.S.A. E-mail: afiege@amnh.org

also influenced to some extent by changes in melt composition, pressure, and temperature (e.g., Kress and Carmichael 1991; Moretti 2005). The Fe oxidation state in natural silicate glasses was determined in several studies, for instance, to understand the  $f_{0}$ , of the mantle sources for basaltic magmas (e.g., Arculus 1985; Kress and Carmichael 1991; Cottrell and Kelley 2011) as well as to determine the kinetics of redox processes based on experimental samples (Gaillard et al. 2003; Magnien et al. 2004, 2008). Considering that even small changes in redox can have a strong effect on melt properties such as the solubility of S, Au, and Cu (e.g., Baker and Moretti 2011; Bell et al. 2011; Simon and Ripley 2011; Zajacz et al. 2012a, 2012b) and that redox effects can be very localized in magmatic/volcanic products (i.e., melt inclusions may be heterogeneous owing to hydrogen loss from a lava after eruption; cf. Christie et al. 1986), the ideal analytical method to understand the kinetics of redox processes in magmatic systems and to determine pre-eruptive redox conditions should have a high spatial resolution and be very precise.

Wet-chemical bulk analyses (e.g., Lange and Carmichael 1989; Schuessler et al. 2008) and Mössbauer spectroscopy (e.g., Botcharnikov et al. 2005; Cottrell et al. 2009; Jayasuriya et al. 2004; Waychunas 1983; Wilke et al. 2002, 2005; Wood and Virgo 1989) facilitate high-precision analyses of the Fe oxidation state in glasses and other Fe-bearing phases; however, in situ analyses with a high spatial resolution are not possible with these methods. Changes in glass color induced by variations in Fe<sup>3+</sup>/ $\Sigma$ Fe can be determined at a high spatial resolution, but they only provide qualitative or potentially semi-quantitative information about the Fe oxidation state (Gaillard et al. 2002, 2003). The analyses of the FeL $\alpha$  peak position (energy) or  $L\beta/L\alpha$  intensity ratios via electron microprobe (EMP) allows a fairly high spatial resolution (5  $\times$  5 um) and an acceptable precision (±2 to 3% absolute), at least for samples containing ≤8 wt% Fe (Höfer et al. 1994, 2000; Fialin et al. 2001). The method reaches its limit of detection at ≤3.5 wt% Fe (Fialin et al. 2001) and, thus, the Fe<sup>3+</sup>/ $\Sigma$ Fe of most intermediate and evolved silicate melt cannot be measured precisely. High beam currents are required for the EMP analyses (about 50-130 nA) and, hence, beam damage can be a major problem when measuring glass samples (Fialin et al. 2001). To prevent beam damage, the samples are either moved during the measurement to minimize impact on a certain area (Höfer et al. 1994) or the beam size is increased significantly (up to 30 µm; Fialin et al. 2001), both limits the spatial resolution of EMP technique. Electron energy loss spectroscopy (EELS) allows high spatial resolution by using a transmission electron microscope, but the sample preparation is difficult (e.g., van Aken et al. 1998, 1999; Garvie and Buseck 1998).

In the last ~15 years, Fe *K*-edge X-ray absorption near-edge structure (XANES) spectroscopy has probably become the most popular method making in situ measurements of the Fe oxidation state in geological materials, as it allows one not only to determine the Fe<sup>3+</sup>/ΣFe ratios in glasses and minerals at very high precision (down to 1%; Cottrell et al. 2009) and at a micrometer scale, but also to estimate the Fe-coordination number (e.g., Wilke et al. 2001). The latter helps to improve our understanding of the structure of silicate melts and glasses and is of significant importance for the interpretation of possible compositional effects on the calibration of the Fe XANES oxidation state method (e.g.,

Botcharnikov et al. 2005; Giuli et al. 2012). Calibrating the Fe u-XANES method for various glass compositions has been the objective of several studies published in the last decade (e.g., Berry et al. 2003; Cottrell et al. 2009; Farges et al. 2004; Galoisy et al. 2001; Giuli et al. 2003, 2011, 2012; Knipping et al. 2015; Wilke et al. 2001, 2004, 2005). The calibration is generally based on the Fe pre-(K-) edge peak in Fe XANES spectra, which is a combination of two or more peaks corresponding to the photon absorption that arises due to a 1s  $\rightarrow$  3d electron transition. The centroid energy of the pre-edge doublet is a function of contributions of the Fe<sup>2+</sup> (at ~7111.5 eV if the analyses was calibrated to 7110.75 eV; see method section) and the  $Fe^{3+}$  (at ~7113.2 eV) in the glass, where the weighted centroid of the doublet changes gradually from Fe<sup>2+</sup>dominated to Fe<sup>3+</sup>-dominated with increasing  $f_{02}$  (see Fig. 1 in Cottrell et al. 2009; and Fig. 3 in Berry et al. 2003). Additionally, the probability of the 1s  $\rightarrow$  3d transition and, thus, of the relative intensities of the peaks in the pre-edge doublet, is a function of the coordination state of Fe in the material being analyzed. With increasing fraction of non-centrosymmetric Fe sites (e.g., tetrahedron), the integrated pre-edge intensity is increasing whereas it is the lowest for regular octahedral sites. In a non-symmetric environment intensity increase is a result of the metal 3d-4p orbital mixing, while in centrosymmetric environments electric dipole transitions are forbidden but, due to quadrupole coupling, weak pre-edge features occur (cf. Wilke et al. 2001, 2005; Berry et al. 2003). Moreover, the Fe-coordination of a quenched glass may depend on the quench rate; i.e., chances to preserve fourfold coordinated Fe during the thermal transition from melt to glass may decrease with decreasing quench rate (Dyar and Birnie 1984; Wilke et al. 2007).

The results of Wilke et al. (2001) and Galoisy et al. (2001) already documented a potential effect of the glass composition on the correlation between the centroid energy of the  $1s\to 3d$  Fe pre-edge peak and the  $Fe^{3+}/\Sigma Fe$  ratio of a glass, indicating a direct link of this effect to differences in  $Fe^{3+}$  coordination. Subsequently, the data of Cottrell et al. (2009) indicated that these differences in centroid energies of basaltic and rhyolitic glasses at a given Fe oxidation state are resolvable via Fe  $\mu\text{-XANES}$ . However, the data set on the calibration of Fe XANES is still somewhat limited, especially for intermediate melt compositions, and the reasons for the possible compositional effect are poorly understood but may be related to changes in Fe-coordination (four-, five-, and sixfold; e.g., Botcharnikov et al. 2005; Berry et al. 2003; Wilke et al. 2001, 2005).

A good understanding of the dependence of the pre-edge feature on melt composition is crucial for accurate determination of the Fe oxidation state in systems with varying melt compositions; e.g., during (chemical) mixing of a felsic and a mafic magma at depth. In this study, we provide new results from Fe μ-XANES measurements on reference glasses with andesitic to rhyolitic composition. In addition, we measured rhyolitic and basaltic reference glasses from Cottrell et al. (2009). These measurements were performed during different sessions and at two different synchrotron radiation sources [Advanced Photon Source (APS), Argonne, U.S.A., and Angströmquelle Karlsruhe (ANKA), Karlsruhe, Germany] to allow an evaluation of the reproducibility of the calibrations and to check for possible differences in calibration with changing beamline setup and beam characteristics (e.g., differences in

photon flux). We re-evaluate the effect of glass composition on the calibration, especially for silicate glasses with intermediate to felsic composition. Moreover, we discuss whether the relationship between centroid energy and Fe oxidation state should be described by a linear regression as suggested by Berry et al. (2003) or by a polynomial function as proposed by Cottrell et al. (2009). The compiled data set will also be used to further improve our understanding of "three-way" relationship between the integrated intensity and the centroid energy of the Fe pre-edge peak as well as the Fe coordination in glasses with rhyolitic to basaltic compositions (cf. Wilke et al. 2001).

#### EXPERIMENTAL AND ANALYTICAL PROCEDURE

# Fe μ-XANES at the 13-ID-E beamline at APS (Argonne)

Micro-XANES spectra were collected on a set of 28 reference glasses with known Fe oxidation state (Table 1). The set of reference glasses comprises 9 hydrous and 5 dry rhyolitic glasses from Moore et al. (1995), 2 hydrous andesitic glasses from Fiege et al. (2014), 2 hydrous dacitic glasses from Bell and Webster (2015), as well as 1 dry rhyolitic and 9 dry basaltic reference glasses from Cottrell et al. (2009). We emphasize that 6 of the glasses prepared by Moore et al. (1995) and the glasses prepared by Cottrell et al. (2009) were already analyzed via Fe XANES (e.g., Cottrell et al. 2009). These 16 glasses were analyzed on 2 samples mounts (NMNH 117393 and NMNH 117436) loaned to us by the Smithsonian Institution (National Museum of Natural History, Washington, D.C., U.S.A.). The bulk valence of most glasses was determined via wet-chemical analyses (method described by Schuessler et al. 2008), while some glasses were analyzed via Mössbauer spectroscopy instead (see Table 1); see, e.g., Wilke et al. (2005).

The analyses were performed at the Advanced Photon Source (APS) of the Argonne National Laboratory (U.S.A.) in 2 sessions. This synchrotron radiation source operates at an energy of 7 GeV and a beam current of 100 mA, at which the electrons are injected into a 1104 m circumference storage ring. The  $\mu$ -XANES analyses were performed at the GSECARS 13-ID-E beamline, which covers an

energy range of 2.4 to 28 keV and allows a high spatial resolution by focusing the beam down to  $2 \times 1~\mu m$  ( $\mu$ -XANES) by using Kirkpatrick-Baez (KB) focusing mirrors (*note*: whenever APS is mentioned hereafter it refers to data collected at the 13-ID-E beamline). The energy of the first-derivative peak of Fe metal foil was calibrated to the Fe *K*-edge energy of 7110.75 eV as determined by Kraft et al. (1996). The spectra were collected in fluorescence mode from 7062 to 7312 eV (total number of points per spectra: 399; counting time per point: 1 s; step size: 5 eV from 7062 to 7107 eV; 0.1 eV from 7107 to 7137 eV (pre-edge region); ~2 eV from 7137 to 7312 eV), using a focused beam ( $2 \times 1~\mu m$ ).

Energy selection was achieved with a Si(111) channel cut monochromator. Notably, the angular divergence of the APS undulators is smaller than the angular acceptance of the crystal reflections, because the beam is strongly collimated. Hence, the energy width of the Fe K-edge peaks is dominated by the natural line-width, even with the Si(111) reflection. Careful measurements at the 13-ID-E beamline showed that the resolution increases only slightly from 0.26 to 0.13 eV when switching from a Si(111) to a Si(311) crystal, while the intensity loss is slightly higher if a Si(311) crystal is used. Thus, the advantage of choosing a Si(311) crystal instead of a Si(111) one is negligible at the APS beamline 13-ID-E.

Three scans were typically performed on each reference glass. Five rhyolitic and two dacitic reference glasses were analyzed during two different sessions at the 13-ID-E beamline to verify reproducibility of our results (see Tables 2 and 3). The hydrous reference glass REV-1 and the dry reference glass VG568 were measured four to five times on the same spot to check for possible irradiation damages (i.e., oxidation or reduction related to extended exposure; total exposure: 40–50 min).

# Fe XANES analyses at the SUL-X beamline at ANKA (Karlsruhe)

All available reference materials were also analyzed at the synchrotron radiation source ANKA (Angströmquelle Karlsruhe) to allow an evaluation of possible differences in the Fe pre-edge feature and its correlation with the Fe oxidation state and the Fe-coordination in the glass that may arise from instru-

<sup>1</sup>Deposit item AM-17-25822, Supplementary Figures and Tables. Deposit items are free to all readers and found on the MSA web site, via the specific issue's Table of Contents (go to http://www.minsocam.org/MSA/AmMin/TOC/2017/Feb2017\_data/Feb2017\_data.html).

TABLE 1. Reference glass materials analyzed via Fe XANES

Composition Sample ID	SiO <sub>2</sub>	TiO <sub>2</sub>	$Al_2O_3$	Fe <sub>2</sub> O <sub>3</sub>	FeO	FeO <sub>tot</sub>	MnO	MgO	CaO	Na₂O	K₂O	$P_2O_5$	SO <sub>3</sub>	CI	H <sub>2</sub> O <sub>tot</sub>	Total	KN/A	Fe³+/ ΣFe	Type of experiment	Citations
Rhyolite																			сиренинени	
DT-18 <sup>a</sup>	72.6	0.25	9.9	3.89	1.80	5.30	N.A.	0.01	0.19	4.76	4.41	N.A.	N.A.	N.A.	±drv	97.81	1.37	0.66	1 atm. exp.	Mo95
DT-29 <sup>a</sup>	73.5	0.25	10.1	5.09	1.10	5.68	N.A.	0.03	0.23	4.14	4.02	N.A.	N.A.	N.A.	,	98.46	1.20		1 atm. exp.	Mo95
DT-31	77.3	0.25	10.5	3.01	1.59	4.30	N.A.	0.03	0.23	3.29	3.33	N.A.	N.A.	N.A.	,	99.53			1 atm. exp.	Mo95
DT-39	73.1	0.26	9.9	1.99	3.89	5.68	N.A.	0.01	0.24	5.01	4.36	N.A.	N.A.	N.A.	,				1 atm. exp.	Mo95
DT-46 <sup>a</sup>	74.4	0.25	10.1	3.58	2.44	5.66	N.A.	0.01	0.24	4.57	4.48	N.A.	N.A.	N.A.	± dry	100.07	1.33	0.569	1 atm. exp.	Mo95
H2O-52	69.9	0.24	9.7	3.43	2.54	5.63	N.A.	0.03	0.24	5.38	4.36	N.A.	N.A.	N.A.	4.18	95.82	1.48	0.549	High-P exp.	Mo95
H2O-53	70.3	0.22	9.5	3.06	2.74	5.49	N.A.	0.02	0.22	5.43	4.35	N.A.	N.A.	N.A.	4.16	95.84	1.52	0.501	High-P exp.	Mo95
H2O-54	71.2	0.24	9.7	3.36	2.36	5.38	N.A.	0.02	0.22	5.41	4.38	N.A.	N.A.	N.A.	3.11	96.89	1.49	0.562	High-P exp.	Mo95
H2O-55	70.7	0.25	9.6	3.59	2.42	5.65	N.A.	0.02	0.22	5.54	4.36	N.A.	N.A.	N.A.	3.30	96.70	1.52	0.572	High-P exp.	Mo95
H2O-63 <sup>a</sup>	70.4	0.23	9.5	3.46	2.11	5.22	N.A.	0.02	0.24	5.22	4.26	N.A.	N.A.	N.A.	4.56	95.44	1.47	0.596	High-P exp.	Mo95
H2O-66	69.7	0.22	8.9	3.05	2.39	5.13	N.A.	0.03	0.17	5.33	4.18	N.A.	N.A.	N.A.	6.04	93.96	1.58	0.535	High-P exp.	Mo95
H2O-67	70.6	0.21	9.0	3.43	2.08	5.17	N.A.	0.02	0.21	5.34	4.18	N.A.	N.A.	N.A.	4.93	95.07	1.56	0.597	High-P exp.	Mo95
REV-1	70.0	0.21	8.8	1.53	3.53	4.91	N.A.	0.02	0.15	5.23	4.16	N.A.	N.A.	N.A.	6.37	93.63	1.57	0.281	High-P exp.	Mo95
REV-3	69.4	0.18	8.7	2.86	2.44	5.01	N.A.	0.03	0.18	5.04	4.07	N.A.	N.A.	N.A.	7.10	92.90	1.55	0.513	High-P exp.	Mo95
VG568 <sup>a</sup>	77.5	0.07	12.52	0.35	1.00	1.31	N.A.	0.03	0.5	3.11	4.57	< 0.01	N.A.	N.A.	±dry	99.65	0.92	0.238	1 atm. exp.	Co09
Dacite																				
PD2K3 <sup>a</sup>	61.69	0.49	15.70	0.64	1.56	2.14	0.09	3.67	4.78	4.34	1.35	0.17	N.A.	< 0.1	5.10°	94.48	0.52	$0.27^{d}$	High-P exp.	Be15
PD2K4 <sup>a</sup>	62.50	0.50	16.03	0.56	1.68	2.18	0.10	3.64	4.72	4.53	1.38	0.17	N.A.	< 0.1	3.99€	95.81	0.53	$0.23^{d}$	High-P exp.	Be15
Andesite																				
AH	61.23	0.85	14.69	1.71	2.98	4.52	0.21	1.34	4.80	3.69	1.69	N.A.	0.32	N.A.	6.61°	100.12	0.53	0.34	High-P exp.	Fi14
SD1	60.91	0.81	14.57	2.02	2.84	4.65	0.22	1.34	4.41	3.49	1.66	N.A.	0.31	N.A.	5.79°	98.36	0.51	0.39	High-P exp.	Fi14
Basalt <sup>b</sup>																				
All (6 glasses	50.8	1.73	16.14	b	b	9.53	N.A.	7.40	11.20	2.75	0.15	0.14	N.A.	N.A.	±dry	99.85	0.25	b,d	1 atm. exp.	Co09
LW (3 glasses	) 49.4	1.94	17.21	b	b	10.17	N.A.	6.13	8.78	3.17	1.50	1.12	N.A.	N.A.	±dry	99.44	0.39	b,d	1 atm. exp.	Co09

Notes: N.A. = Not analyzed.  $H_2O_{tot}$  = 100% EMP Total; NK/A = (Na+K)/Al mass ratio. Citations: Be15 (Bell and Webster 2015); Fi14 (Fiege et al. 2014); Mo95 (Moore et al. 1995); Co09 (Cottrell et al. 2009). More details about the reference glasses are given in Supplementary¹ Table A.1 and A.2. and A.2. Analyzed during two XANES session at APS.

<sup>&</sup>lt;sup>b</sup> The analyzed basaltic reference glasses (AII\_-35, AII\_0, AII\_05, AII\_15, AII\_25, AII\_45; LW\_-20, LW\_-10, LW\_10) cover a Fe<sup>3+</sup>/ΣFe ratio of 0.035 to 0.611; see Supplementary<sup>1</sup> Tables A.1 and A.2.

<sup>&</sup>lt;sup>c</sup> Measured by NIR spectroscopy.

d Measured by Mössbauer spectroscopy; all other Fe³+/ΣFe values were determined via wet-chemical analyses (e.g., Schuessler et al. 2008), the error Fe³+/ΣFe values is ≤0.02.

mental differences. At ANKA the electrons are injected with an energy of 2.5 GeV and an initial current of up to 150 mA into a 100.4 m circumference storage ring. The XANES analyses were performed at the SUL-X beamline, which uses a wiggler as radiation source, covering an energy range of 2.4 to 21 keV (note: whenever ANKA is mentioned hereafter it refers to data collected at the SUL-X beamline). The beam can be focused down to  $50 \times 50$  µm by using KB mirrors combined with decreasing of an intermediate focus by a slit system. We used a rectangular spot size of about  $200 \times 150 \mu m$  to improve counting statistics (note: the sample size was sufficient for a larger beam). The energy of the first-derivative peak of Fe metal foil was calibrated to the Fe K-edge energy of 7112 eV and corrected to 7110.75 eV (Kraft et al. 1996) after the analyses to allow direct comparison to the results obtained at APS. The spectra were collected in fluorescence mode from 6992 to 7493 eV [total number of points per spectra: 344; counting time per point: 4 s in the pre-edge region and 1 s for all other energies; step size: 5 and 2 eV from 7062 to 7108 eV; 0.15 eV from 7108 to 7118 eV (pre-edge region); 0.25 eV from 7118 to 7142 eV (edge); step size was increased continuously from 1.1 to 3.8 eV in the energy range from 7142 to 7493; these energy values are related to 7112 eV for the K-edge of Fe metal foil]. At ANKA a Si(311) crystal pair was used in the fixed exit double crystal monochromator to achieve a higher energy resolution. In comparison with the Si(311) crystal pair used at ANKA SUL-X beamline the energy resolution of Si(111) channel cut at the APS 13-ID-E beamline is somewhat lower as can be seen in the smoother and often broader features in the Fe K XANES spectra (see Supplementary<sup>1</sup> Material A).

Each glass was analyzed at least twice and on the reference materials REV-1 and VG568 sequences of 4–5 scans (10 min per scan) were performed on the same spot to check for possible changes in Fe oxidation state with increasing exposure to the beam (i.e., to exclude radiation damages that may lead to an oxidation or reduction). The two dacitic (PD2K3 and PD2K4) reference glass samples were analyzed during two sessions (2015.2 and 2015.3) to verify reproducibility.

In addition, two crystalline model compounds with different Fe oxidation state and Fe coordination (siderite:  $Fe^{2+}$ , sixfold coordination; Fe-bearing sanidine:  $Fe^{3+}$ , fourfold) were analyzed in transmission mode at the SUL-X beamline of ANKA to test the end-member positions in the coordination plot (variogram), which was developed by Wilke et al. (2001) and further constrained by, e.g., Giuli et al. (2003); see Results section.

#### Data processing

The raw data were dead-time corrected and the software Athena (Ifeffit package; Newville 2001) was used to perform a self-absorption (SA) correction and to pre-edge/post-edge normalize the spectra. The SA correction is necessary because the spectra were collected in fluorescence mode (in/out angle: 45°; see also Tröger et al. 1992). The SA correction was performed by using the FLUO algorithm (developed by Daniel Haskel; Argonne National Laboratory, U.S.A.) in combination with the known glass composition. Cottrell et al. (2009) observed that SA has a negligible effect on the centroid energy of the pre-edge peak, while the influence of SA on the integrated intensity of the pre-edge peak is quite significant.

We emphasize that the fluorescence mode was selected owing to the samples properties, which often did not allow transmission mode. This procedure is supposedly beneficial for the applicability of the resulting calibrations since fluorescence mode is often required for the analyses of natural samples (especially melt inclusions). Similarly, a 45° in/out angle was chosen owing to technical limitation of some beamlines to position the sample normal to the beam, which would minimize SA (Tröger et al. 1992).

The pre-edge peak was fit from ~7082 to ~7119 eV following the procedure described by Cottrell et al. (2009) and using the program Fityk (Wojdyr 2010). We used an exponentially modified Gaussian and an arctangent function to fit the background first and, subsequently we added two Gaussians to fit the (background corrected) pre-edge peak (see Supplementary<sup>1</sup> Fig. A.1). Fityk provides all relevant information, such as the intensity, the integrated area and the center position/energy for the Gaussians. The area and the center position were used to calculate the centroid energy of the pre-edge peak for each analysis. The energies of the XANES results obtained at ANKA (calibrated on 7112.0 eV) were shifted by -1.25 eV to fit the calibration used for the measurements at APS (calibrated on 7110.75 eV). This fitting approach differs slightly from previously proposed procedures (cf. Wilke et al. 2001) and is, in our opinion, more user-friendly than earlier published methods. We emphasize that, no matter which fitting approach is applied, a very good fit of the background in the energy range of ~7108 to ~7117 eV is crucial to obtain accurate results for the Fe oxidation state and coordination.

#### RESULTS AND DISCUSSION

The Fe XANES spectra collected on the reference glasses confirm the non-crystalline state of the samples (for details about the samples see Moore et al. 1995; Cottrell et al. 2009; Fiege et al. 2014; Bell et al. 2015), whereas minor quench-related effects on the Fe-coordination cannot be ruled out (Wilke et al. 2006; see full spectra of REV-1, VG568, PD2K3, and AH in Supplementary<sup>1</sup> Fig. A.1). The results obtained during different sessions at APS and ANKA are presented and compared in Figure 1a-1d. A comparison of the reference glass measurements of the first (2014.1) and the second (2014.3) XANES session at the 13-ID-E beamline at APS reveals an excellent session-to-session reproducibility (Fig. 1b), except for one outlier (marked by a red circle in Figs. 1a and 1b), which will be excluded for any following discussion and interpretation. Similarly, the centroid energies determined for the dacitic reference glasses PD2K3 and PD2K4 based on XANES spectra collected at the SUL-X beamline at ANKA differ by ≤0.06 eV from session to session; i.e., the centroid energy is reproduced within  $2\sigma$  uncertainty (see Supplementary<sup>1</sup> Material B). The results of the Fe XANES analyses on the reference glasses are given in Supplementary<sup>1</sup> Tables B.1 (APS data) and B.2 (ANKA data).

The shape of the pre-edge peak measured at APS is typically smoother than the shape of the pre-edge peaks collected at ANKA (see Fig. 2 and Supplementary Material A) that often show more distinctively two peaks. This is likely related to the different monochromator crystals used for the analyses (Cottrell et al. 2009). However, the centroid positions are largely unaffected by this effect, i.e., the centroid energies determined based on XANES spectra collected at ANKA and APS, respectively, are often identical within  $2\sigma$  and the absolute difference is <0.1 eV for 12 of the 19 felsic glasses, which were analyzed at both synchrotron sources (see, e.g., Figs. 1d and 3a). The felsic reference materials DT-18, DT-31, H2O-63, and H2O-67. PD2K4, AH, and SD1 differ by 0.11 to 0.20 eV between ANKA and APS; however, they still follow the same trend. The results obtained at ANKA and APS, respectively for the basaltic reference materials differ typically by 0.11–0.20 eV (see Supplementary<sup>1</sup> Material B). Independent of the glass composition, the centroid energies obtained at ANKA are generally a little higher (Fig. 1d); however, all results are still identical within the estimated overall uncertainty of the analytical method (±0.1 eV).

In Figures 3b–3d, we compare our reference glass analyses to the results from some of the most comprehensive works that determined the centroid energy of the Fe pre-edge peak in XANES spectra collected on silicate glasses with known Fe oxidation state. The previously published centroid energies for different silicate glass compositions (rhyolitic to basaltic) were all corrected to match our energy calibration of the first derivative peak of Fe metal foil (7110.75 eV). We emphasize that this correction is necessary and a common procedure to allow comparison between data sets using different energies for the first-derivative peak of Fe metal foil. It is remarkable that the centroid positions determined by Berry et al. (2003) on anorthitediopside glasses and by Cottrell et al. (2009) on rhyolitic and basaltic glasses are about 1 eV lower than the centroid energies determined in the present study, as well as the studies of Giuli et al. (2011, 2012) and Wilke et al. (2005) for glasses with rhyolitic

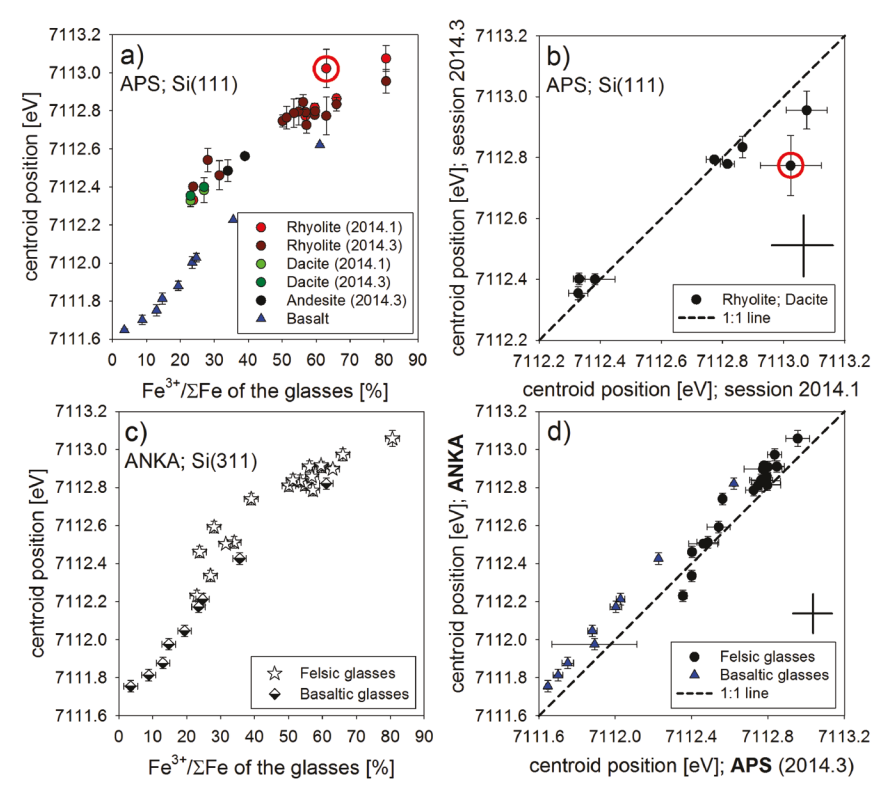


FIGURE 1. (a–d) Result of the Fe XANES analyses on rhyolitic and basaltic reference glasses. (a) Centroid energy of the Fe pre-edge peak vs. Fe oxidation state in the glass; APS data only. (b) Reproducibility of the centroid energies from session (2014.1) to session (2014.3). (c) Centroid energy vs. Fe oxidation state in the glass; ANKA data only. (d) Comparison of the centroid energies determined for the felsic and basaltic references glasses based on XANES spectra collected at APS and ANKA, respectively. The Fe oxidation states of the reference glasses were typically determined by wet chemistry and in three cases by Mössbauer spectroscopy (see Table 2). The error of the Fe<sup>3+</sup>/ $\Sigma$ Fe ratios is  $\pm 2\%$ . The black cross in the lower right corner of b and d represents the overall uncertainty of the method ( $\pm 0.1$  eV). To distinguish trends/symbols see online color version.

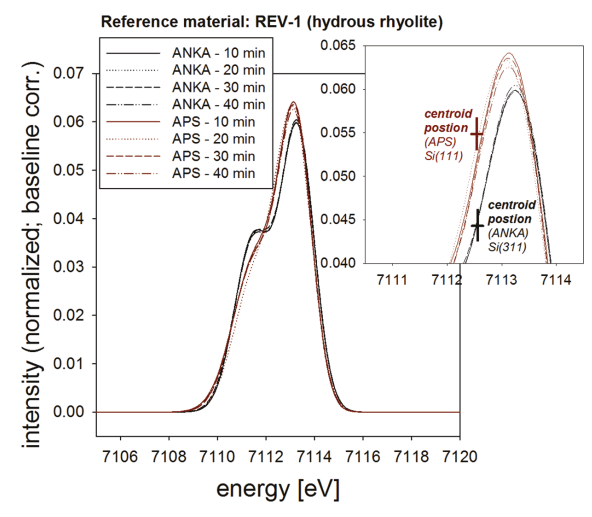


FIGURE 2. Fe XANES pre-edge peak of REV-1 measured at APS and ANKA. A sequence of 4 analyses on the same spot was performed to show that irradiation damages can be ruled out. Such sequences were also performed on other reference materials and all of the sequences show that oxidation or reduction related to extended exposure to the X-ray beam can be ruled out (see also Supplementary¹ Fig. A.1). The widths of the crosses marking the centroid energies represent the overall uncertainty of the analytical method (±0.1 eV). To distinguish trends/symbols see online color version.

to basaltic composition; see Figures 3c and 3d. This shift seems to be largely independent of the melt composition and on the Fe oxidation state in the glass. A shift of 1 eV in the centroid energy cannot be explained by a poor fit of the spectra, which mainly affects the integrated intensity of the pre-edge peak but, based on our experience, results typically in differences of << 0.1 eV for the centroid energy. Notably, our set of analyses includes all of the rhyolitic glasses and most of the basaltic glasses measured by Cottrell et al. (2009). We cannot rule out that instrumental differences between, e.g., the X26A beamline at NSLS (used by Cottrell et al. 2009) and 13-ID-E at APS or SUL-X at ANKA are responsible for the shift and the only way to clarify this is to measure the full set of references glasses also at NSLS (and potentially at the 20B beamline at KEK, High Energy Accelerator Research Organization, Tsukuba, Japan; used by Berry et al. 2003). However, considering that we measured similar centroid energies for basaltic, andesitic, dacitic, and rhyolitic reference glasses at two different synchrotron sources (APS and ANKA; see Fig. 1) using two different monochromator crystals [Si(111) and Si(311)] and that our centroid energies are consistent with other previous results shown in Figure 3, another possible explanation for the ~1 eV shift of the data provided by Berry et al. (2003) and Cottrell et al. (2009) when compared to all other results considered in this study is that some not identified differ-

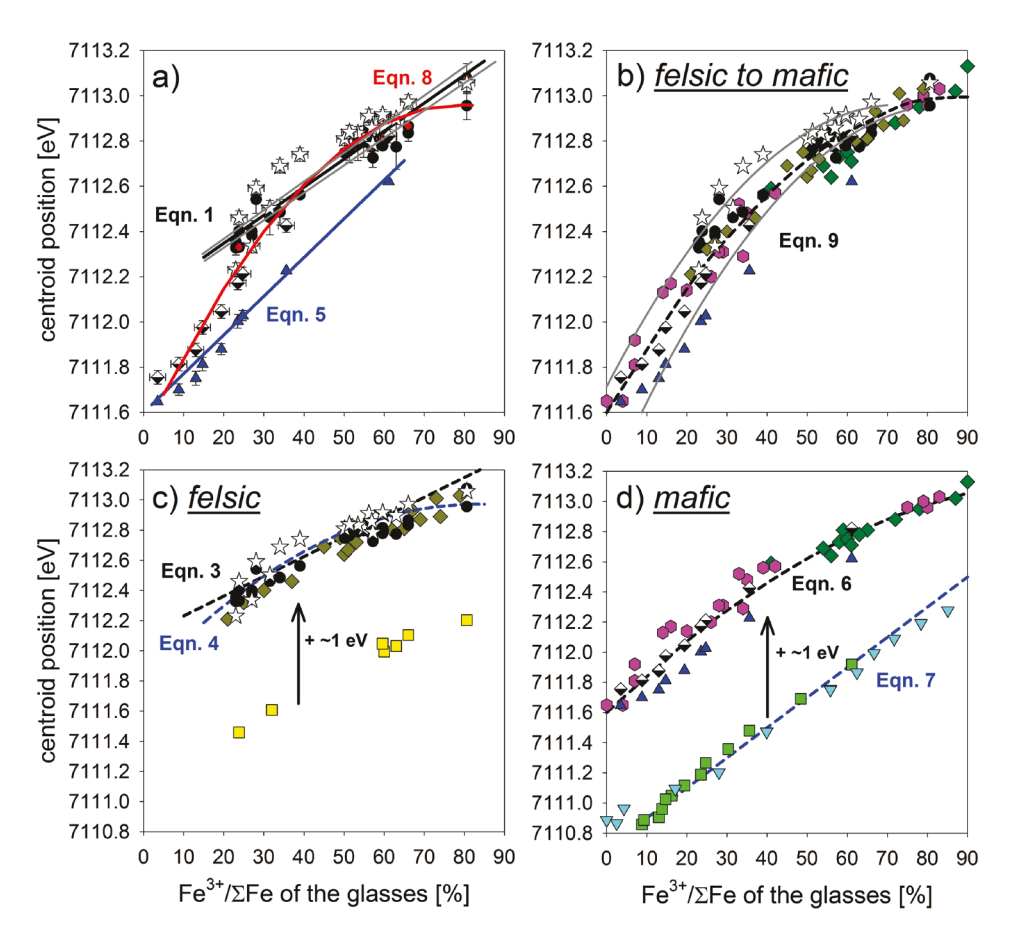


FIGURE 3. (a–d) Calibration trends for the determination of the Fe oxidation state in glasses based on the centroid energy of the Fe pre-edge peak. (a) Only results from this study. The felsic glasses cover a range of compositions from dacitic andesite to rhyolite. The red crosses are analyses from another session (the outlier marked in Fig. 1 is excluded). The gray lines provide an example for the determined uncertainties for the individual equations (here, trends are plotted for Eq. 1). (b) Reference glass data from three previous studies and from this study. The plotted data set covers glass compositions ranging from felsic to mafic and Fe XANES spectra were collected at four different synchrotron radiation sources (APS, ANKA, ESRF, DESY). The results of Berry et al. (2003) and Cottrell et al. (2009) are excluded (see text for details). The gray lines reflect trends for ±6% Fe³+/ΣFe. At least 64% of the compiled data with <60% Fe³+/ΣFe are covered by this range. Here, the 64% are a minimum value since the individual uncertainties are not considered. Notice that Fe³+/ΣFe ratios of ≥60% in magmas are rare (Carmichael 1991). (c) Comparison of results from Fe XANES analyses on felsic glasses performed at different synchrotron radiation sources (APS, ANKA, ESRF, NSLS). (d) Comparison of results from Fe XANES analyses on mafic glasses performed at different beamlines at different synchrotron radiation sources (13-ID-E at APS, SUL-X at ANKA, ID26 at ESRF, X26A at NSLS, L at DESY, 20B at KEK). *Notes:* \* The centroid energies provided in the literature were corrected (*corr.*) to match our energy calibration (i.e., 7110.75 eV for the first derivative peak of a XANES spectrum collected on Fe metal foil). The regressions were predicted using KaleidaGraph and the displayed trends were labeled according to the numbering of the equations given in the text. # A Si(111) four-crystal monochromator was used by Wilke et al. (2005), which should have a similar energy resolution as most Si(311) double crystal setups. To distin

ences exist in the calibrations for the energy of the first derivative peak of Fe metal foil ( $E_{\text{Fe-metal}}$ ). While such an explanation cannot be tested, it is in agreement with the fact that the literature data presented by Cottrell et al. (2009) in their Figure 10 (e.g., Wilke et al. 2005; Métrich et al. 2006) was taken from the tables in those references without accounting for differences in  $E_{\text{Fe-metal}}$  between their study and some of the previously published results.

Irradiation damage can be ruled out as a reason for the 1 eV shift because up to five consecutive analyses on the same spot on reference glass produced identical spectra (examples are

given in Fig. 2 and in Supplementary<sup>1</sup> Fig. A.1). Furthermore, oxidation (or reduction) of the iron in a glass related to a strong X-ray beam should affect mainly reduced (or oxidized) to intermediate samples but should have a negligible effect on almost fully oxidized (or reduced) samples. Thus, if a higher photon flux density would affect the  $Fe^{3+}/\Sigma Fe$  valence ratio in the glass one would expect a different slope for the different trends in Figure 3 instead of the observed consistent offset by 1 eV. This is further confirmed by the good correlation between the data collected at the relatively low photon flux beamline SUL-X at

ANKA and the data obtained at the GSECARS 13-ID-E beamline at APS that operates at an approximately four orders of magnitude higher photon flux density [rough estimation of the photon fluxes for the applied analytical conditions: 13-ID-E (APS):  $\sim$ 5 × 10<sup>16</sup> photons/s/100 mA/mm<sup>2</sup> vs. SUL-X (ANKA):  $\sim$ 1 × 10<sup>12</sup> photons/s/100 mA/mm<sup>2</sup>]. Similarly, it is worth noting that hydrous glasses are typically more prone to irradiation damages than anhydrous glasses (observed for sulfur by Wilke et al. 2008) and our personal experience with XANES analyses at S K-edge indicate that primitive (basaltic) glasses are more prone to beam damage than evolved (rhyolitic) glasses. The correlation between bulk composition (incl. H<sub>2</sub>O) and the susceptibility to irradiation damages would result in scattering of the results presented, e.g., in Figure 3, which is not observed and, thus, confirms the absence of a detectable irradiation damage during our Fe XANES analyses. The absence of detectable irradiation damages during Fe XANES analyses of silicate glasses is also consistent with previous results for soda-lime silicate glasses, observing decreasing photo-reduction effects with increasing Fe content in the glass, resulting in minor irradiation damages at ~0.45 wt% FeO (Ferreira et al. 2013). However, we emphasize that the set of analyzed reference materials does not include hydrous mafic glasses (only nominally dry basalts were measured) and, thus, it cannot be evaluated if hydrous mafic glasses are prone to beam damage during analyses at certain synchrotron beamlines. Given the shift by -1 eV of the centroid energies determined by Berry et al. (2003) and Cottrell et al. (2009), we will treat these two data sets separately in the following discussion.

# Fe μ-XANES calibrations

In this section, we provide several equations for the calculation of the Fe oxidation state of glasses based on Fe XANES measurement. We emphasize that each equation should only be applied for the range of Fe<sup>3+</sup>/ $\Sigma$ Fe covered by the set of data used to calculate the individual trends (e.g., Eq. 1:  $0.85 \ge \text{Fe}^{3+}/\Sigma$ Fe  $\ge 0.3$ ).

The centroid energy determined at APS for the Fe pre-edge peak  $C_{Fe}$  (eV) and the Fe<sup>3+</sup>/ $\Sigma$ Fe ratio (%) of felsic glasses containing 60.9 to 77.5 wt% SiO<sub>2</sub> (dacitic andesite to rhyolite) and a total FeO (FeO<sub>tot</sub>) of ~2.1 to ~5.7 wt% follow a linear trend (Eq. 1; Fig. 3a):

$$C_{Fe}$$
 [eV] = 0.012395 (±0.00026217) ×  
Fe<sup>3+</sup>/ $\Sigma$ Fe + 7112.1 (±0.014525); R<sup>2</sup> = 0.987 (1) (linear; felsic glasses; only APS data from this study).

Whereas a second-order polynomial function provides a slightly better fit (Eq. 2; not plotted):

$$C_{Fe}$$
 [eV] = 7111.9 (±0.04005) + 0.021332 (±0.0019789) ×  $Fe^{3+}/\Sigma Fe$  = 0.00010344 (±2.2705e-5) ×  $(Fe^{3+}/\Sigma Fe)^2$ ; (2) (polynomial; felsic glasses; only APS data from this study).

These and the following regressions were fit using the software KaleidaGraph, applying the locally weighted least-squared error method and a 2 $\sigma$  error for the centroid energy. The standard error [= (standard deviation)/(square route of the number of data points)] is provided for each constant. Notably, Cottrell et al. (2009) and Wilke et al. (2005) proposed two different secondorder polynomial functions for their Fe XANES data, while Berry et al. (2003) suggested a linear fit.

If the reference glass data from this study (APS and ANKA) and the measurements on rhyolite glasses by Giuli et al. (2012) are combined (assuming an error of 0.05 eV for the centroid energy provided by Giuli et al. 2012), the following linear fit is predicted (Eq. 3; Fig. 3c):

$$C_{Fe}$$
 [eV] = 0.013128 (±0.00011251) × Fe<sup>3+</sup>/ $\Sigma$ Fe + 7112.1 (±0.00591); R<sup>2</sup> = 0.972 (3) [linear; felsic glasses; this study: APS and ANKA (Fe<sup>3+</sup>/ $\Sigma$ Fe  $\ge$  0.3); Giuli et al. 2012]

Equation 3 may only be used for glasses with  $Fe^{3+}/\Sigma Fe \ge 0.3$ , considering the differences between the ANKA and the APS data at  $Fe^{3+}/\Sigma Fe < 0.3$ . A second-order polynomial function provides again a slightly better fit (Eq. 4; Fig. 3c).

$$C_{Fe}$$
 [eV] = 7111.8 (± 0.027548) + 0.028279 (±0.0013348)  
× Fe<sup>3+</sup>/ $\Sigma$ Fe - 0.00017065 (±1.498e-5) × (Fe<sup>3+</sup>/ $\Sigma$ Fe)<sup>2</sup>;  
R<sup>2</sup> = 0.976 (4)  
(polynomial; felsic glasses; this study: APS and ANKA; Giuli et al. 2012).

The similar  $R^2$  values of the Equations 1 through 4 indicate that the correlation between  $Fe^{3+}/\Sigma Fe$  and  $C_{Fe}$  for felsic glasses can be accurately described by both a linear trend and a second-order polynomial function. The good correlation between our rhyolite data and the results of Giuli et al. (2012) suggests that an accurate determination of  $Fe^{3+}/\Sigma Fe$  of unknown felsic glasses based on Fe XANES performed at the synchrotron sources APS (using the 13-ID-E beamline), ANKA (SUL-X) or ESRF (ID26) requires only a limited set of reference glass measurements to check against our calibration(s) (Eqs. 3 or 4).

The basaltic reference glasses measured at APS reveal a linear relationship between Fe<sup>3+</sup>/ $\Sigma$ Fe and C<sub>Fe</sub> (Fig. 3a):

$$\begin{split} &C_{Fe}\left[eV\right] = 0.017125 \ (\pm 0.00016824) \\ &\times Fe^{3+} / \Sigma Fe + 7111.6 \ (\pm 0.0060138); \ R^2 = 0.996 \\ &\text{(linear; basaltic glasses; only APS data from this study)}. \end{split} \tag{5}$$

Cottrell et al. (2009) reported data for these reference materials and proposed a polynomial function. However, a linear trend is consistent with the results of Berry et al. (2003) for similar glass compositions. Consistent with these contradictory interpretations by previous studies we observe that the combined data set for mafic glasses (41.6 to 53.0 wt% SiO<sub>2</sub>; 6.3 to 14.5 wt% FeO<sub>tot</sub>) plotted in Figure 3d (Wilke et al. 2005; Giuli et al. 2011; this study) can be described by a linear or a second-order polynomial trend, since both regressions have similar  $R^2$  values. Here, we only present the second-order polynomial regression (Fig. 3d):

$$\begin{split} &C_{Fe}\left[eV\right] = 7111.6 \; (\pm 0.034497) + 0.025722 \; (\pm 0.0019192) \\ &\times Fe^{3+}/\Sigma Fe - 0.00010624e\text{--}5 \; (\pm 2.0847e\text{--}5) \times (Fe^{3+}/\Sigma Fe)^2, \\ &R^2 = 0.980 \end{split} \tag{6}$$

(polynomial; mafic glasses; this study: APS and ANKA; Wilke et al. 2005; Giuli et al. 2011).

This equation can be used to calculate Fe<sup>3+</sup>/ $\Sigma$ Fe based on XANES spectra collected on mafic glasses at the 13-ID-E beamline at APS (this study), the ID26 at ESRF (Giuli et al. 2011) and the A1 at DESY (Deutsches Elektronen-Synchrotron, Hamburg, Wilke et al. 2005).

The combined results of Cottrell et al. (2009 collected at the X26A beamline at NSLS) and Berry et al. (2003; 20B beamline at KEK) for mafic glasses can also be described by a linear or a second-order polynomial regression, while only the linear equation and trend are presented (Eq. 7; Fig. 3d). However, as mentioned above, the data of Cottrell et al. (2009) and Berry et al. (2003) may be influenced by unknown differences in the energy calibration and, thus, the regression may need to be shifted by +1 eV and should only be applied with caution.

$$C_{Fe}$$
 [eV] = 0.019989 (±6.5459e-5) × Fe<sup>3+</sup>/ $\Sigma$ Fe + 7110.7 (±0.0016786); R<sup>2</sup> = 0.994 (7) (linear; mafic glasses; Berry et al. 2003; Cottrell et al. 2009).

Interestingly, the difference between felsic and mafic glasses is small. For instance, the data obtained at the SUL-X beamline at ANKA for basaltic, andesitic, dacitic, and rhyolitic glasses is fairly well described by a polynomial trend (Eq. 8; Fig. 1c and 3a):

$$C_{\text{Fe}}$$
 [eV] = 7111.5 (±0.068488) + 0.037062 (±0.0038309)   
×Fe<sup>3+</sup>/ΣFe - 0.00023527 (±4.6679e-5)×(Fe<sup>3+</sup>/ΣFe)<sup>2</sup>;   
R<sup>2</sup> = 0.973 (8) (polynomial; all ANKA data from this study).

For measurements performed at the 13-ID-E beamline at APS, a similar correlation can be observed if the results for the basaltic glasses AII\_25 and AII\_45 are not considered. The centroid energies AII\_25 and AII\_45 show an offset of ~0.25 eV and ~0.18 eV, respectively, when compared to the ANKA data.

More intriguingly, the entire data set (this study; Giuli et al. 2011, 2012; Wilke et al. 2005) is fairly well described by a single second-order polynomial equation (Fig. 3b), if the results of Cottrell et al. (2009) and Berry et al. (2003) are excluded:

$$C_{Fe}$$
 [eV] = 7111.6 (±0.03443) + 0.030638 (±0.0016853)  
× Fe<sup>3+</sup>/ $\Sigma$ Fe - 0.00016656 (±1.8254e-5) × (Fe<sup>3+</sup>/ $\Sigma$ Fe)<sup>2</sup>;  
R<sup>2</sup> = 0.964 (9)

(polynomial; all data from this study: ANKA and APS; Giuli et al. 2011, 2012; Wilke et al. 2005].

Here, ~64% of the data with Fe³+/ $\Sigma$ Fe < 60% is reproduced within ±6% Fe³+/ $\Sigma$ Fe (see gray lines in Fig. 3b). At Fe³+/ $\Sigma$ Fe ≥60%; however, such Fe oxidation states require very oxidizing conditions (typically >QFM+3; see Fig. 4a in Fiege et al. 2015), which are rarely realized in magmatic systems (cf. Carmichael 1991). The relatively good correlation of Equation 9 with the compiled data (R² = 0.964) indicates once again that potential beam damages have a negligible effect on  $C_{Fe}$  for the investigated range of compositions, since beam damage would modify Fe³+/ $\Sigma$ Fe to different extents depending, e.g., on glass composition (incl. H<sub>2</sub>O), photon flux and exposure time [see also results of Wilke et al. (2008) for S XANES]. The differences between

the data we collected at the SUL-X at ANKA and our analyses performed at the 13-ID-E at APS for felsic glasses with Fe<sup>3+</sup>/ $\Sigma$ Fe < 0.3 (Figs. 3a and 3c) indicate that a second-order polynomial function may be favored for the results of analyses with Si(311) crystals, while a linear function is preferred when Si(111) crystals were used as monochromator (Fig. 3a). This effect might be related to the small differences in energy resolution when comparing spectra obtained by using Si(311) crystals to those collected using Si(111) crystals. However, this observation is mainly based on the results of three reference material (PD2K3, PD2K4, and VG568) and has to be interpreted with caution, considering the good correlation found for all other samples (see Fig. 1d and text). Importantly, the possible effect of Si(311) crystals vs. Si(111) crystals is in agreement with the linear trend proposed by Berry et al. (2003), who used Si(111) monochromator crystals and with the second-order polynomial function proposed, e.g., by Cottrell et al. (2009), who used Si(311) crystals. However, the results obtained by Wilke et al. (2005) indicate that at Fe<sup>3+</sup>/  $\Sigma \text{Fe} < 0.15$  a polynomial function might be more suitable at least for analyses using a Si(111) four crystal monochromator that yields probably a similar energy resolution as most Si(311) double crystal setups (Fig. 3d).

To conclude, there is a very good session-to-session reproducibility and the good correlation between centroid energies obtained at different beamlines of different synchrotron radiation sources, indicates that the provided equations (except for Eq. 7) can typically be used for measurements at any synchrotron radiation source. In other words, differences in instrumentation have probably a negligible effect on the calibration. However, for specialized applications aiming at superior precision we recommend to measure a limited set of reference glasses to check against our calibrations. The compositional influence on the calibration is also small (see Fig. 3b), therefore, Equation 9 is applicable to XANES spectra collected on silicate glass with compositions ranging from rhyolite to basalt, at an arbitrary beamline. However, Equation 9 only provides a first-order approximation of the Fe<sup>3+</sup>/ $\Sigma$ Fe ratio (uncertainty  $\geq$ 6% absolute for Fe<sup>3+</sup>/ $\Sigma$ Fe < 60%) and, thus, the specific equations provided above for data sets collected at the 13-ID-E beamline (APS) and the SUL-X beamline (ANKA), respectively, on felsic samples and basaltic samples, respectively, are favored due to their higher R<sup>2</sup> values.

### Fe-coordination in basaltic and rhyolitic glasses

The intensity of the Fe pre-edge peak is mostly influenced by the Fe-coordination symmetry in the analyzed compound (e.g., Farges 2001; Wilke et al. 2005). The coordination of ferric and ferrous iron in crystalline materials is typically very well defined. Several previous studies determined the integrated peak intensities and centroid energies of the Fe pre-edge peak in XANES spectra collected on mineral phases with different Fe-coordinated and oxidation state (e.g., powdered fayalite, siderite, staurolite, or andradite; e.g., Westre et al. 1997; Giuli et al. 2003; Wilke et al. 2001, 2004, 2005). A variogram (originally constructed by Wilke et al. 2001) based on the integrated peak intensities and the centroid energies of the model compounds can be used to evaluate the oxidation state and coordination of Fe in glasses. In Figure 4 we compare our results from the reference glass analyses performed at the 13-ID-E beamline at APS with previously

published results (Berry et al. 2003; Botcharnikov et al. 2005; Giuli et al. 2011, 2012; Wilke et al. 2005), while the results we obtained at the SUL-X beamline at ANKA are plotted together with the APS data in Figure 5. It is worth noting that the centroid energies and integrated intensities determined by Wilke et al. (2001) based on analyzed crystalline model compounds (using transmission mode) at the ID26 beamline at ESRF and at the IV-1 beamline at the Stanford Synchrotron Radiation Laboratory (SSRL, U.S.A.) are consistent with those obtained by Farges (2001) at the beamline IV-I at SSRL and by Giuli et al. (2003) at the beamline BM-8 at ESRF (both studies used fluorescence mode). Hence, the variogram proposed by Wilke et al. (2001) can probably be used without additional in-session analyses of crystalline model compounds. The XANES spectra we collected on siderite and sanidine at the SUL-X beamline (ANKA) confirm this observation (Fig. 4a; see also Supplementary<sup>1</sup> Table B.3). For clarity, we set the first derivative peak of Fe metal foil to 0 eV like in Giuli et al. (2003) for all data displayed in Figure 4 and 5; e.g., 7110.8 eV were subtracted from the centroid energies of Wilke et al. (2005). Comparison of results obtained during the two session at the 13-ID-E beamline at APS reveal a slight session-to-session drift (average difference in integrated peak intensity is ~0.038, see Supplementary<sup>1</sup> Table B.1) providing a rough constraint on the session-to-session reproducibility for the applied method (fluorescence mode combined with SA correction using the FLUO algorithm).

The results show that the ferric iron in felsic glasses is most likely fourfold coordinated, while, at the first view, ferrous iron

seems to be fivefold coordinated (Fig. 4b). This observation is in agreement with previous studies (e.g., Farges 2001; Farges et al. 2004; Giuli et al. 2012). However, according to Wilke et al. (2005), no distinction is possible between a mixture of fourfold- and sixfold-coordinated iron and the possible occurrence of fivefold iron in the glass structure. On the other hand, Giuli et al. (2012) suggested based on previous observations (e.g., Giuli et al. 2002, 2003, 2011) that ferrous iron is rarely, if ever, predominantly sixfold coordinated in the studied glasses, indicating that Fe<sup>2+</sup> in our felsic glasses and the rhyolitic glasses of Giuli et al. (2012) is on average fivefold coordinated. Farges et al. (2004) suggested a linear correlation between centroid energy and integrated intensity, while Giuli et al. (2012) proposes a nonlinear relationship. The compiled data set shown in Figure 4 is not sufficient for a definite interpretation; however, it supports a linear correlation.

Giuli et al. (2012) further suggested that the changes in the (K+Na)/Al (KN/A) mass ratio (from 1.1 to 1.9) can explain slight differences in the coordination-oxidation trends observed for rhyolitic glasses. However, the KN/A mass ratios of our rhyolites vary from 0.9 to 1.6 and the dacitic and andesitic glasses have a KN/A of ~0.5. All glasses (except probably for the andesitic ones) seem to follow the same trend in the variogram. For instance, the spectra collected at APS on the "reduced" samples PD2K4 and VG568 (Fe³+/ $\Sigma$ Fe ~ 0.23) show integrated intensities (~0.164) and centroid energies of the Fe pre-edge peak that are identical within error (~7112.38 eV; data of session 2014.3), while their KN/A ratio differs significantly (0.53 and 0.92, respectively).

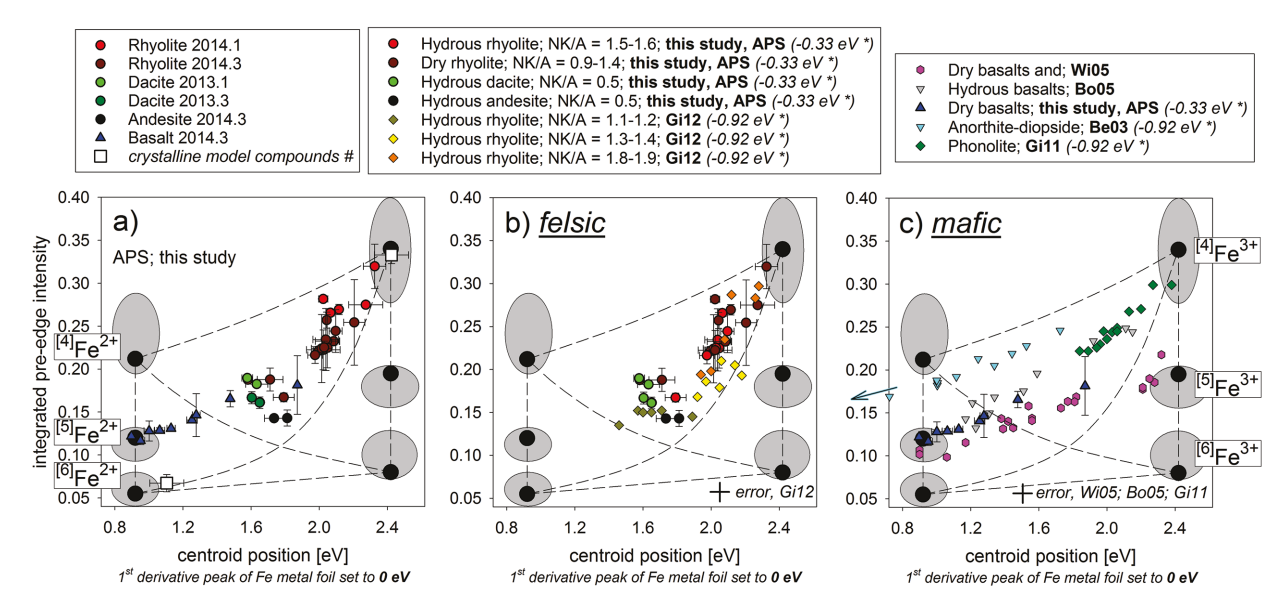


FIGURE 4. (a-c) Dependence of the Fe-coordination on the Fe oxidation state and the glass composition. This coordination plot (variogram) was developed by Wilke et al. (2001). For the end-members (purely fourfold-, fivefold-, and sixfold-coordinated ferrous and ferric iron) we used the peak intensities and the centroid energies that were determined by Wilke et al. (2001; black circles; collected in transmission mode) and by Giuli et al. (2003; gray ellipses; collected in fluorescence mode) for various crystalline compounds (see text). These values are consistent with results for Fe model compounds obtained by Farges (2001). (a) Only results from this study (rhyolitic to basaltic glass compositions; APS data only) are shown. (b) Result from this study for felsic reference glasses (rhyolite to dacitic andesite; APS data only) are compared to results from Giuli et al. (2012; Gi12) for rhyolite. (c) Results from this study for basaltic glasses (APS data only) are plotted in comparison to XANES data for mafic glasses provided by Berry et al. (2003; Be03), Botcharnikov et al. (2005; Bo05), Wilke et al. (2005; Wi05), and Giuli et al. (2011; Gi11). Notes: 2014.1/2014.3: Two different XANES sessions at the APS. NK/A = (Na+K)/Al mass ratio of the glass. To distinguish trends/symbols see online color version.

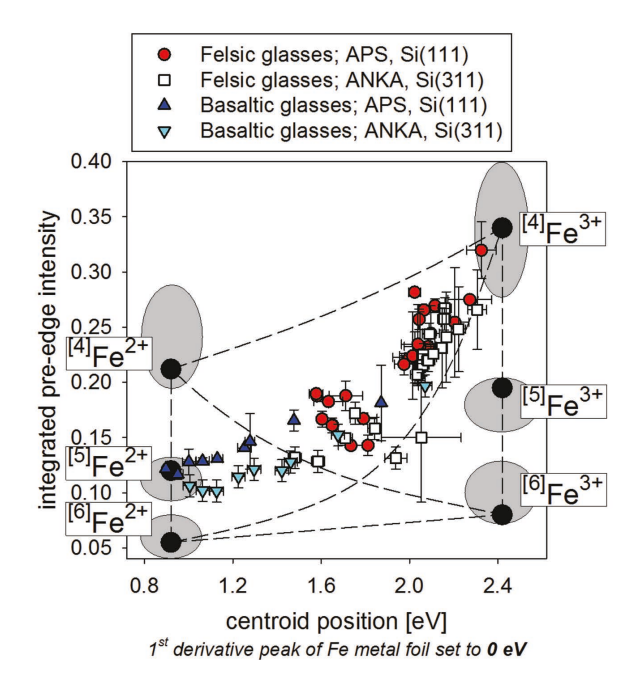


FIGURE 5. Variogram showing the results obtained at the 13-ID-E beamline at APS and at the SUL-X beamline at ANKA for felsic and basaltic reference materials. This coordination plot (variogram) was developed by Wilke et al. (2001). To distinguish trends/symbols see online color version.

Similar observations can be made for more oxidizing conditions (compare results for DT-31 and H2O-63 obtained at APS and ANKA). Hence, we cannot confirm a dependence of the Fe-coordination on KN/A; our data perhaps suggest that the influence of KN/A in felsic systems is negligible, considering that the integrated intensities for several glasses with different KN/A but similar centroid energies are identical within uncertainty.

The results for basaltic glass follow less steep trends in the variogram (Fig. 4c). The peak intensities of the different studies vary quite significantly for a given centroid energy. However, our results are similar or even identical within uncertainty with the data obtained by Wilke et al. (2005), confirming that our analytical and data processing procedure (incl. SA correction) yields accurate results (incl. the values for the integrated intensity), since Wilke et al. (2005) collected their spectra in transmission mode (i.e., no SA correction required; cf. Tröger et al. 1992). Moreover, the results from each of the five studies shown in Figure 4c seem to follow a trend, which is parallel to the trends indicated by the results of the other studies.

Giuli et al. (2011) measured their XANES spectra in fluorescence mode, but a SA correction is not mentioned within the manuscript, which might explain the higher integrated intensities determined for phonolite when compared to our results for basalt. Similarly, Botcharnikov et al. (2005) mentioned difficulties with the SA correction of their analyses and, thus, their integrated intensities are probably too high. The results of Berry et al. (2003) shown in Figure 4c are difficult to evaluate, owing to the 1 eV shift toward lower centroid energies as discussed above; however, the data points are certainly following similar trends. Notably, even if the Berry et al. (2003) data is shifted

by +1 eV, the integrated intensities for a given centroid energy are still higher than those obtained by this study and by Wilke et al. (2005). Again, self-absorption effects that can result in an artificially high intensity of the pre-edge peak cannot be ruled out, because the glass samples were measured in fluorescence mode a SA correction procedure is not mentioned in the work of Berry et al. (2003). We emphasize that quench related changes in the pre-edge feature can be ruled out as a possible explanation for the elevated intensities observed by Berry et al. (2003), Botcharnikov et al. (2005), and Giuli et al. (2011) since quench effects would result in lower values for the integrated peak intensity (Wilke et al. 2006). In contrast to felsic glasses, none of the basaltic glasses may contain sixfold coordinated Fe only. Considering only results that were either SA corrected (this study) or collected in transmission mode (i.e., no SA effect; Wilke et al. 2005), the Fe in basaltic glasses seems always to be present as a mixture of different coordination, which remains constant with changing oxidation state and is on average close to a fivefold coordination (Fig. 4c and 5).

The fact that most analyses of reference material at APS and ANKA show integrated intensities that are similar or even higher than those of model compounds with fivefold-coordinated Fe indicates that sixfold-coordinated Fe may not be present in silicate glasses. Although the data set does not allow to fully rule out the contribution of sixfold-coordinated Fe, considering that some of the spectra collected at ANKA reveal intensities that indicate a slight contribution of sixfold Fe. Moreover, changes in coordination related to differences in quench rate may affect the coordination in both rhyolitic and basaltic systems. Dyar and Birnie (1984) noted that denser glasses (e.g., basalts) are more prone to structural changes during quenching than less dense glasses (e.g., rhyolite), taking the direct relationship between cooling rate and density into account. The authors suggest that fourfold-coordinated iron can transition to sixfold iron during quenching. However, the smooth trends observed by various studies for mafic glass compositions in a variogram (Fig. 4c) indicate that quench related changes are probably minor, considering that different techniques were used for the preparation of the glasses (e.g., high-P vs. 1 atm synthesis; see Table 1), which yield different quench rates. Thus, we suggest that the Fe XANES spectra collected on rapidly quenched glasses can also be used for the interpretation of the Fe coordination in silicate melts. This observations is mostly in agreement with observation made by Wilke et al. (2007) based on in situ Fe XANES measurements on simple silicate melts, suggesting that the local structural environment around Fe in silicate glasses is similar to that in the melt.

The observed changes in Fe-coordination with changing Fe oxidation state in felsic systems have important implications for the effect of  $f_{\rm O2}$  on melt polymerization and, thus, on melt viscosity. While fourfold-coordinated (tetrahedral) Fe is acting as a polymerizing network unit, at least in peralkaline felsic melts, fivefold (or sixfold) Fe is probably acting as a depolymerizing network modifier. The constant fourfold/fivefold (or fourfold/sixfold) ratios observed in basaltic systems indicate that  $f_{\rm O2}$  has a negligible effect on the polymerization and, thus, on the viscosity of basaltic melts. These interpretations are in agreement with previous works, noting that ferric and ferrous iron are typically

network modifiers and only alkali metals can stabilize ferric iron in a network forming (fourfold) tetrahedral coordination (e.g., Mysen et al. 1980).

#### **IMPLICATIONS**

Iron XANES analyses are frequently used, for instance, to determine (pre-eruptive) redox conditions based on the measurement of quenched melt inclusions (e.g., Kelley and Cottrell 2009), to elucidate the kinetics of (magmatic) redox processes (e.g., Magnien et al. 2004, 2008) and to further understand the role of melt composition on Fe coordination in silicate melts (e.g., Giuli et al. 2012). In this study we performed Fe  $\mu$ -XANES measurements at two different beamlines (13-ID-E at APS; SUL-X at ANKA) on a large set of reference glasses with basaltic to rhyolitic composition to re-evaluate this technique. We compared our results to existing data and there are six main outcomes, which have important implications for the application of the Fe XANES method:

- (1) We show for the first time results of Fe XANES analyses performed at different synchrotron radiation sources on a set of 19 felsic and 9 basaltic reference glasses and we compare our results to literature data. The compiled data set shows that changes in instrumentation have a probably negligible effect on the correlation between the centroid energy of the Fe pre-edge peak and the Fe<sup>3+</sup>/ $\Sigma$ Fe of the glass.
- (2) The correlation between the centroid energy and  $Fe^{3+}/\Sigma Fe$  can often be described accurately by both linear and by second-order polynomial functions; compare also Cottrell et al. (2009) to Berry et al. (2003). The data set shows that the compositional effect on the centroid energy of the Fe pre-edge peak at a given Fe oxidation state is small (e.g., Eq. 9,  $R^2 = 0.964$ ; see also Fig. 2b). However, using specific empirical equations for specific glass compositions will yield a higher precision.
- (3) We provide equations for different glass compositions and we suggest that these equations can be applied after a small set of in-session standard analyses and accurate energy calibration (on Fe metal foil).
- (4) We show that an extended exposure to synchrotron radiation does not lead to a detectable change of the Fe oxidation state in the studied silicate glasses, even at the high photon flux density at the GSECARS 13-ID-E beamline (APS, Argonne), which is approximately four orders of magnitude higher than at the settings of the SUL-X beamline (ANKA, Karlsruhe).
- (5) Consistent with previous observations, our data show that the Fe-coordination in felsic glasses changes with Fe oxidation state; most likely from fivefold in reduced glasses to fourfold in oxidized glasses, while basaltic glasses are characterized by a mixture of fivefold and fourfold iron, which remains fairly constant with changing redox conditions. This has important implications for the effect of redox on melt structure/viscosity.
- (6) This study confirms previous works recognizing that the effect of bulk composition on the Fe coordination in glasses is recorded by changes in the integrated inten-

sity of the Fe pre-edge peak, while the centroid energy remains almost unaffected by variations in composition/Fe coordination as mentioned previously (see bullet point 2).

#### ACKNOWLEDGMENTS

This project was supported by a U.S. National Science Foundation Collaborative Research grant to Adam Simon (EAR 1250239) and Philipp Ruprecht (EAR 1250414). This research used resources of the Advanced Photon Source, a U.S. Department of Energy (DOE) Office of Science User Facility operated for the DOE Office of Science by Argonne National Laboratory under Contract No. DE-AC02-06CH11357. We acknowledge the Synchrotron Light Source ANKA for provision of instruments at their beamline SUL-X.

# REFERENCES CITED

- Arculus, R.J. (1985) Oxidation status of the mantle—past and present. Annual Review of Earth and Planetary Sciences, 13, 75–95.
- Baker, D.R., and Moretti, R. (2011) Modeling the solubility of sulfur in magmas: a 50-year old geochemical challenge. Reviews in Mineralogy and Geochemistry, 73, 167–213.
- Bell, A.S., and Webster, J.D. (2015) Dissolved Cl, oxygen fugacity, and their effects on Fe behavior in a hydrous rhyodacitic melt. American Mineralogist, 100, 1595–1599
- Bell, A., Simon, A., and Guillong, M. (2011) Gold solubility in oxidized and reduced, water saturated mafic melt. Geochimica et Cosmochimica Acta, 75, 1718–1732.
- Berry, A.J., O'Neill, H.St.C., Jayasuriya, K.D., Campbell, S.J., and Foran, G.J. (2003) XANES calibrations for the oxidation state of iron in a silicate glass. American Mineralogist, 88, 967–977.
- Botcharnikov, R.E., Koepke, J., Holtz, F., McCammon, C., and Wilke, M. (2005) The effect of water activity on the oxidation and structural state of Fe in a ferro-basaltic melt. Geochimica et Cosmochimica Acta, 69, 5071–5085.
- Carmichael, I.S. (1991) The redox states of basic and silicic magmas: a reflection of their source regions? Contributions to Mineralogy and Petrology, 106, 129–141.
- Christie, D.M., Carmichael, I.S., and Langmuir, C.H. (1986) Oxidation states of mid-ocean ridge basalt glasses. Earth and Planetary Science Letters, 79, 397–411.
- Condie, K.C. (1993) Chemical composition and evolution of the upper continental crust: contrasting results from surface samples and shales. Chemical Geology, 104 1–37
- Cottrell, E., and Kelley, K.A. (2011) The oxidation state of Fe in MORB glasses and the oxygen fugacity of the upper mantle. Earth and Planetary Science Letters, 305, 270–282.
- Cottrell, E., Kelley, K.A., Lanzirotti, A., and Fischer, R.A. (2009) High-precision determination of iron oxidation state in silicate glasses using XANES. Chemical Geology, 268, 167–179.
- Dyar, M.D., and Birnie, D.P. (1984) Quench media effects on iron partitioning and ordering in a lunar glass. Journal of Non-Crystalline Solids, 67, 397–412.
- Farges, F. (2001) Crystal chemistry of iron in natural grandidierites: An X-ray absorption fine-structure spectroscopy study. Physics and Chemistry of Minerals, 28, 619–629.
- Farges, F., Lefrère, Y., Rossano, S., Berthereau, A., Calas, G., and Brown, G.E. (2004) The effect of redox state on the local structural environment of iron in silicate glasses: a combined XAFS spectroscopy, molecular dynamics, and bond valence study. Journal of Non-Crystalline Solids, 344, 176–188.
- Ferreira, P.G., de Ligny, D., Lazzari, O., Jean, A., Gonzalez, O.C., and Neuville, D.R. (2013) Photoreduction of iron by a synchrotron X-ray beam in low iron content soda-lime silicate glasses. Chemical Geology, 346, 106–112.
- Fialin, M., Wagner, C., Métrich, N., Humler, E., Galoisy, L., and Bézos, A. (2001) Fe<sup>3+</sup>/ΣFe vs. FeLα peak energy for minerals and glasses: Recent advances with the electron microprobe. American Mineralogist, 86, 456–465.
- Fiege, A., Behrens, H., Holtz, F., and Adams, F. (2014) Kinetic vs. thermodynamic control of degassing of H<sub>2</sub>O–S ± Cl-bearing andesitic melts. Geochimica et Cosmochimica Acta, 125, 241–264.
- Fiege, A., Holtz, F., Behrens, H., Mandeville, C.W., Shimizu, N., Crede, L.S., and Goettlicher, J. (2015) Experimental investigation of the S and S-isotope distribution between H<sub>2</sub>O-S±Cl fluids and basaltic melts during decompression. Chemical Geology, 393, 36–54.
- Gaillard, F., Scaillet, B., and Pichavant, M. (2002) Kinetics of iron oxidation-reduction in hydrous silicic melts. American Mineralogist, 87, 829–837.
- Gaillard, F., Schmidt, B., Mackwell, S., and McCammon, C. (2003) Rate of hydrogeniron redox exchange in silicate melts and glasses. Geochimica et Cosmochimica Acta, 67, 2427–2441.
- Galoisy, L., Calas, G., and Arrio, M.A. (2001) High-resolution XANES spectra of iron in minerals and glasses: Structural information from the pre-edge region. Chemical Geology, 174, 307–319.
- Garvie, L.A.J., and Buseck, P.R. (1998) Ratios of ferrous to ferric iron from nanometer sized areas in minerals. Nature, 396, 667–670.
- Giuli, G., Pratesi, G., Cipriani, C., and Paris, E. (2002) Iron local structure in tektites and impact glasses by extended X-ray absorption fine structure and high-

- resolution X-ray absorption near edge structure spectroscopy. Geochimica et Cosmochimica Acta, 66, 4347–4353.
- Giuli, G., Paris, E., Pratesi, G., Koeberl, C., and Cipriani, C. (2003) Iron oxidation state in the Fe-rich layer and silica matrix of Libyan Desert Glass: A high-resolution XANES study. Meteoritics & Planetary Science, 38, 1181–1186.
- Giuli, G., Paris, E., Hess, K.U., Dingwell, D.B., Cicconi, M.R., Eeckhout, S.G., Fehr, K.T., and Valenti, P. (2011) XAS determination of the Fe local environment and oxidation state in phonolite glasses. American Mineralogist, 96, 631–636.
- Giuli, G., Alonso-Mori, R., Cicconi, M.R., Paris, E., Glatzel, P., Eeckhout, S.G., and Scaillet, B. (2012) Effect of alkalis on the Fe oxidation state and local environment in peralkaline rhyolitic glasses. American Mineralogist, 97, 468–475.
- Höfer, H.E., Brey, G.P., Schulz-Dobrick, B., and Oberhänsli, R. (1994) The determination of the oxidation state of iron by the electron microprobe. European Journal of Mineralogy, 6, 407–418.
- Höfer, H.E., Weinbruch, S., McCammon, C.A., and Brey, G.P. (2000) Comparison of two electron probe microanalysis techniques to determine ferric iron in synthetic wüstite samples. European Journal of Mineralogy, 12, 63–71.
- Hofmann, A.W. (1988) Chemical differentiation of the Earth: The relationship between mantle, continental crust, and oceanic crust. Earth and Planetary Science Letters, 90, 297–314.
- Jayasuriya, K.D., O'Neill, H.St.C., Berry, A.J., and Campbell, S.J. (2004) A Mössbauer study of the oxidation state of Fe in silicate melts. American Mineralogist, 89. 1597–1609.
- Kelley, K.A., and Cottrell, E. (2009) Water and the oxidation state of subduction zone magmas. Science, 325, 605–607.
- Knipping, J.L., Behrens, H., Wilke, M., Göttlicher, J., and Stabile, P. (2015) Effect of oxygen fugacity on the coordination and oxidation state of iron in alkali bearing silicate melts. Chemical Geology, 411, 143–154.
- Kraft, S., Stümpel, J., Becker, P., and Kuetgens, U. (1996) High resolution X-ray absorption spectroscopy with absolute energy calibration for the determination of absorption edge energies. Review of Scientific Instruments, 67, 681–687.
- Kress, V.C., and Carmichael, I.S.E. (1991) The compressibility of silicate liquids containing Fe<sub>2</sub>O<sub>3</sub> and the effect of composition, temperature, oxygen fugacity and pressure on their redox states. Contributions to Mineralogy and Petrology, 108, 82–92.
- Lange, R.A., and Carmichael, I.S. (1989) Ferric-ferrous equilibria in Na<sub>2</sub>O-FeO-Fe<sub>2</sub>O<sub>3</sub>-SiO<sub>2</sub> melts: Effects of analytical techniques on derived partial molar volumes. Geochimica et Cosmochimica Acta, 53, 2195–2204.
- Magnien, V., Neuville, D.R., Cormier, L., Mysen, B.O., Briois, V., Belin, S., Pinet, O., and Richet, P. (2004) Kinetics of iron oxidation in silicate melts: a preliminary XANES study. Chemical Geology, 213, 253–263.
- Magnien, V., Neuville, D.R., Cormier, L., Roux, J., Hazemann, J.L., de Ligny, D., Pascarelli, S., Vickridge, I., Pinet, O., and Richet, P. (2008) Kinetics and mechanisms of iron redox reactions in silicate melts: The effects of temperature and alkali cations. Geochimica et Cosmochimica Acta, 72, 2157–2168.
- Métrich, N., Susini, J., Foy, E., Farges, F., Massare, D., Sylla, L., Lequien, S., and Bonnin-Mosbah, M. (2006) Redox state of iron in peralkaline rhyolitic glass/ melt: X-ray absorption micro-spectroscopy experiments at high temperature. Chemical Geology, 231, 350–363.
- Moore, G., Righter, K., and Carmichael, I.S.E. (1995) The effect of dissolved water on the oxidation state of iron in natural silicate liquids. Contributions to Mineralogy and Petrology, 120, 170–179.
- Moretti, R. (2005) Polymerisation, basicity, oxidation state and their role in ionic modelling of silicate melts. Annals of Geophysics, 48, 583–608.
- Mysen, B.O., Seifert, F., and Virgo, D. (1980) Structure and redox equilibria of ironbearing silicate melts. American Mineralogist, 65, 867–884.
- Newville, M. (2001) EXAFS data analysis program Athena. Journal of Synchrotron Radiation, 8, 322.
- O'Connor, J.T. (1965) A classification for quartz-rich igneous rocks based on feldspar ratios. U.S. Geological Survey Professional Paper B, 525, 79–84.
- Schuessler, J.A., Botcharnikov, R.E., Behrens, H., Misiti, V., and Freda, C. (2008)

- Oxidation state of iron in hydrous phono-tephritic melts. American Mineralogist, 93, 1493–1504.
- Simon, A., and Ripley, E. (2011) The role of magmatic sulfur in the formation of ore deposits. Reviews in Mineralogy and Geochemistry, 73, 513–578.
- Tröger, L., Arvanitis, D., Baberschke, K., Michaelis, H., Grimm, U., and Zschech, E. (1992) Full correction of the self-absorption in soft-fluorescence extended X-ray-absorption fine structure. Physical Review B, 46(6), p.3283.
- van Aken, P.A., Liebscher, B., and Styrsa, V.J. (1998) Quantitative determination of iron oxidation states in minerals using Fe L<sub>2/3</sub>-edge electron energy-loss near edge structure spectroscopy. Physics and Chemistry of Minerals, 25, 323–327.
- van Aken, P.A., Styrsa, V.J., Liebscher, B., Woodland, A.B., and Redhammer, G.J. (1999) Microanalysis of Fe<sup>3+</sup>/ΣFe in oxide and silicate minerals by investigation of electron energy-loss near-edge structures (ELNES) at the Fe M<sub>23</sub> edge. Physics and Chemistry of Minerals, 26, 584–590.
- Waychunas, G.A. (1983) Mössbauer, EXFAS and X-ray diffraction study of Fe<sup>3+</sup> clusters in MgO:Fe and magnesiowüstite (Mg,Fe)<sub>1-x</sub>O: Evidence for specific cluster geometries, Journal of Materials Science, 18, 195–207.
- Westre, T.E., Kennepohl, P., DeWitt, J.G., Hedman, B., Hodgson, K.O., and Solomon, E.I. (1997) A multiplet analysis of Fe K-edge 1s → 3d pre-edge features of iron complexes. Journal of the American Chemical Society, 119, 6297–6314.
- Wilke, M., Farges, F., Petit, P.-E., Brown, G.E. Jr., and Martin, F. (2001) Oxidation state and coordination of Fe in minerals: an Fe K XANES spectroscopic study. American Mineralogist, 86, 714–730.
- Wilke, M., Behrens, H., Burkhard, D.J., and Rossano, S. (2002) The oxidation state of iron in silicic melt at 500 MPa water pressure. Chemical Geology, 189, 55–67.
- Wilke, M., Partzsch, G.M., Bernhardt, R., and Lattard, D. (2004) Determination of the iron oxidation state in basaltic glasses using XANES at the K-edge. Chemical Geology, 213, 71–87.
- Wilke, M., Partzsch, G.M., Bernhardt, R., and Lattard, D. (2005) Erratum: Determination of the iron oxidation state in basaltic glasses using XANES at the K-edge. Chemical Geology, 220, 143–161.
- Wilke, M., Schmidt, C., Farges, F., Malavergne, V., Gautron, L., Simionovici, A., Hahn, M., and Petit, P.E. (2006) Structural environment of iron in hydrous aluminosilicate glass and melt-evidence from X-ray absorption spectroscopy. Chemical Geology, 229, 144–161.
- Wilke, M., Farges, F., Partzsch, G.M., Schmidt, C., and Behrens, H. (2007) Speciation of Fe in silicate glasses and melts by in-situ XANES spectroscopy. American Mineralogist. 92, 44–56.
- Wilke, M., Jugo, P.J., Klimm, K., Susini, J., Botcharnikov, R., Kohn, S.C., and Janousch, M. (2008) The origin of S<sup>4+</sup> detected in silicate glasses by XANES. American Mineralogist, 93, 235–240.
- Wojdyr, M. (2010) Fityk: a general-purpose peak fitting program. Journal of Applied Crystallography, 43, 1126–1128.
- Wood, B.J., and Virgo, D. (1989) Upper mantle oxidation state: Fe<sup>3+</sup> iron contents of lherzolite spinels by <sup>57</sup>Fe Mössbauer spectroscopy and resultant oxygen fugacities. Geochimica et Cosmochimica Acta, 53, 1277–1291.
- Zajacz, Z., Candela, P.A., Piccoli, P.M., and Sanchez-Valle, C. (2012a) The partitioning of sulfur and chlorine between andesite melts and magmatic volatiles and the exchange coefficients of major cations. Geochimica et Cosmochimica Acta, 89, 81–101.
- Zajacz, Z., Candela, P.A., Piccoli, P.M., Wälle, M., and Sanchez-Valle, C. (2012b) Gold and copper in volatile saturated mafic to intermediate magmas: Solubilities, partitioning, and implications for ore deposit formation. Geochimica et Cosmochimica Acta, 91, 140–159.

MANUSCRIPT RECEIVED APRIL 20, 2016 MANUSCRIPT ACCEPTED AUGUST 29, 2016 MANUSCRIPT HANDLED BY SASA BAJT

# **Erratum**

Calibration of Fe XANES for high-precision determination of Fe oxidation state in glasses: Comparison of new and existing results obtained at different synchrotron radiation sources by A. Fiege, P. Ruprecht, A.C. Simon, A.S. Bell, J. Göttlicher, M. Newville, T. Lanzirotti, and G. Moore (February, vol. 102, p. 369–380, 2017. Article DOI: http://dx.doi.org/10.2138/am-2017-5822. Erratum DOI: https://doi.org/10.2138/am-2017-E102410.)

Figure 3 of this article was published without the key to the symbols used. We have the corrected figure below.

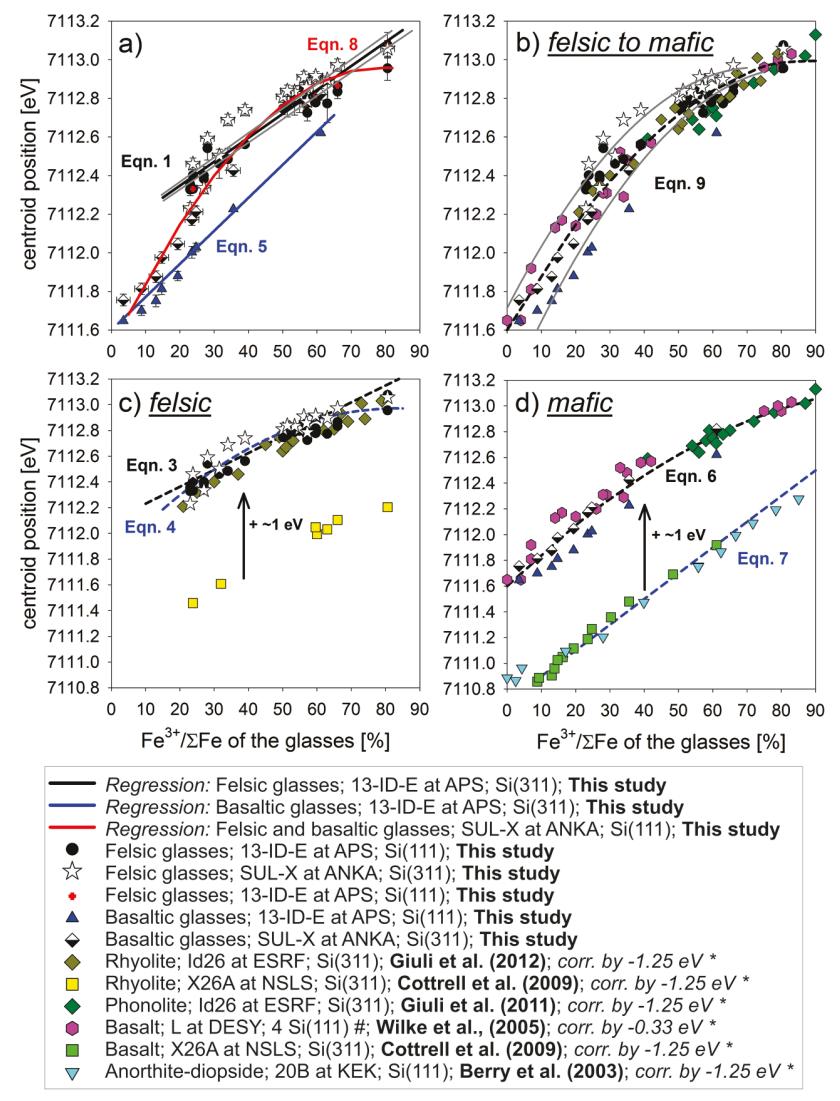


FIGURE 3. (a–d) Calibration trends for the determination of the Fe oxidation state in glasses based on the centroid energy of the Fe pre-edge peak. (a) Only results from this study. The felsic glasses cover a range of compositions from dacitic andesite to rhyolite. The red crosses are analyses from another session (the outlier marked in Fig. 1 is excluded). The gray lines provide an example for the determined uncertainties for the individual equations (here, trends are plotted for Eq. 1). (b) Reference glass data from three previous studies and from this study. The plotted data set covers glass compositions ranging from felsic to mafic and Fe XANES spectra were collected at four different synchrotron radiation sources (APS, ANKA, ESRF, DESY). The results of Berry et al. (2003) and Cottrell et al. (2009) are excluded (see text for details). The gray lines reflect trends for ±6% Fe³+/ΣFe. At least 64% of the compiled data with <60% Fe³+/ΣFe are covered by this range. Here, the 64% are a minimum value since the individual uncertainties are not considered. Notice that Fe³+/ΣFe ratios of ≥60% in magmas are rare (Carmichael 1991). (c) Comparison of results from Fe XANES analyses on felsic glasses performed at different synchrotron radiation sources (APS, ANKA, ESRF, NSLS). (d) Comparison of results from Fe XANES analyses on mafic glasses performed at different beamlines at different synchrotron radiation sources (13-ID-E at APS, SUL-X at ANKA, ID26 at ESRF, X26A at NSLS, L at DESY, 20B at KEK). *Notes:* \* The centroid energies provided in the literature were corrected (*corr.*) to match our energy calibration (i.e., 7110.75 eV for the first derivative peak of a XANES spectrum collected on Fe metal foil). The regressions were predicted using KaleidaGraph and the displayed trends were labeled according to the numbering of the equations given in the text. # A Si(111) four-crystal monochromator was used by Wilke et al. (2005), which should have a similar energy resolution as most Si(311) double crystal setups. To disti